https://doi.org/10.48048/tis.2022.4587

Structural Dynamics and Susceptibility of Anti-Alzheimer's Drugs Donepezil and Galantamine against Human Acetylcholinesterase

Bodee Nutho*, Somchai Yanarojana and Porntip Supavilai

Department of Pharmacology, Faculty of Science, Mahidol University, Bangkok 10400, Thailand

(*Corresponding author's e-mail: bodee.nut@mahidol.ac.th)

Received: 8 March 2021, Revised: 14 June 2021, Accepted: 14 July 2021

Abstract

Alzheimer's disease (AD) is a major public health problem worldwide due to an increase in the elderly population. The current pharmacotherapy for the early stages of AD is mainly dependent on cholinesterase inhibitors. Two of the most commonly used anti-AD drugs, donepezil (DPZ) and galantamine (GLM), are selective inhibitors for human acetylcholinesterase (*h*AChE). However, the inhibitory activity of DPZ on *h*AChE was more potent than GLM by ~85 times. To better understand the molecular basis for differences in mode of inhibition of *h*AChE by both drugs, molecular dynamics (MD) simulation was performed. The results showed that the active site residues of *h*AChE/DPZ had the higher hydrogen bond occupancies as compared to *h*AChE/GLM. Nevertheless, the 2 drugs directly formed hydrogen bonds with the catalytic residue H447 of *h*AChE. The per-residue free energy decomposition suggested that DPZ interacted with the residues in peripheral anionic site of *h*AChE, resulting in the greater binding affinity of DPZ than that of GLM toward *h*AChE. The binding free energy calculation based on MM-PBSA and MM-GBSA methods indicated that van der Waal interactions played a predominant role as the driving force for binding process of DPZ and GLM to *h*AChE. Moreover, the predicted total binding free energy of *h*AChE/DPZ was stronger than *h*AChE/GLM, which was consistent well with the experimental data. We hope that our findings provide useful information for further design of novel *h*AChE inhibitors.

Keywords: Binding free energy, Donepezil, Galantamine, Human acetylcholinesterase, Molecular dynamics simulations

Introduction

Alzheimer's disease (AD) is one of the most common causes of dementia associated with an irreversible neurodegenerative brain disorder. AD is estimated about 60 - 80 % of all dementia cases in elderly population over the age of 65 [1]. The progression of disease results in severe memory loss, cognitive impairment and behavioral changes [2]. These symptoms interfere the normal daily lifestyle and quality of life of individual patients. Although the etiology of AD remains unclear, it is believed to involve some important risk factors, including advance age, family history and heredity [3-5]. Currently, the neuropathologic hallmarks of disease have been well described and established. They are linked to the accumulation of abnormal proteins, consisting of senile plaques and neurofibrillary tangles (NFTs). The former type is the result of the aggregation of extracellular toxic amyloid-β (Aβ) peptide, while the latter one is related to the intracellular accumulation of paired helical filaments (PHF) of hyperphosphorylated form of microtubule-associated tau protein [6,7]. The depositions of either senile plaques or abnormal tau protein are capable to activate neurotoxic cascades and decrease the rate of interconnection between neurons, leading to a synaptic dysfunction and followed by neuronal cell death [8]. The studies have been found that a significant loss of cholinergic neurons was normally present in AD brain [9]. As a result, the incapability of cholinergic transmission with remarkable decline of acetylcholine (ACh), which is known as an important neurotransmitter in learning, memory and cognition, can lead to AD symptoms [10]. Therefore, one of the rationales for AD treatment is to reduce the rate of ACh breakdown by inhibiting enzyme acetylcholinesterase (AChE) that plays a crucial role in hydrolysis of ACh into choline and acetate. Based on this strategy, most of current drugs for AD treatment have been used as AChE inhibitors (AChEIs) [11]. To date, AChEIs have been approved by the U.S. Food and Drug Administration (FDA) for symptomatic treatment of AD, namely DPZ (Aricept®), GLM (Razadyne®),

rivastigmine (Exelon®) and tacrine (Cognex®) [12]. Unfortunately, tacrine is not used widely clinically because of a high incidence of hepatotoxicity and its poor tolerability [13]. Moreover, these drugs might be limited for clinical uses due to the excessive activation of cholinergic system at peripheral sites, leading to an occurrence of some peripheral side effects [14]. Thus, the newer compounds with the high potency and low undesired side effects need to be further discovered and designed.

With a view to design novel compounds from currently available anti-AD drugs, DPZ is a non-competitive, rapidly reversible, and selective inhibitor of AChE in the brain [15,16]. Whereas GLM acts as a reversible, competitive, and selective inhibitor of AChE. In addition, GLM is able to enhance the cholinergic activity *via* the allosteric modulation of nicotinic ACh receptor, thereby potentiating the receptor activity in response to ACh [17]. For the pharmacological effect, DPZ and GLM are suitable for inhibition of AChE with low toxicity [14,18]. The chemical structures of both drugs are shown in **Figure 1**.

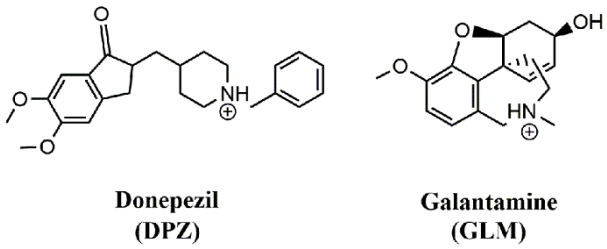

Figure 1 Chemical structures of DPZ and GLM. Note that the tertiary amine of DPZ and GLM is protonated at physiological pH.

Structural insight on human AChE (*h*AChE, EC 3.1.1.7, **Figure 2**) showed that the hydrophobic active site of *h*AChE, termed as catalytic anionic site (CAS) is approximately located 20 Å deep in the bottom of a narrow gorge [19]. This cavity could be divided into 4 subsites, named from the interactions between ACh and each region as following: (*i*) anionic subsite is involved in amino acid residue W86. This residue plays an important role in the stabilization of trimethyl ammonium group of ACh via cation-π interaction [20]; (*ii*) oxyanion hole is formed by backbone –NH– groups of amino acids G121, G122 and A204. This area is associated with the accommodation of ACh carbonyl oxygen forming a transient tetrahedral AChE/ACh complex [21]; (*iii*) acyl binding pocket composes of aromatic amino acids phenylalanine (F295, F297 and F338), which bind to acyl group of ACh [22]; (*iv*) esteratic site contains 3 key amino acid residues (S203, E334 and H447) [20], which is known to be a catalytic triad and participates in catalytic reaction. At the rim of the gorge, it is also involved in another important binding site, namely peripheral anionic site (PAS), consisting set of aromatic residues (Y72, D74, Y124, W286, Y337 and Y341), where it is thought to be an initial binding site of AChE/ACh complex [23].

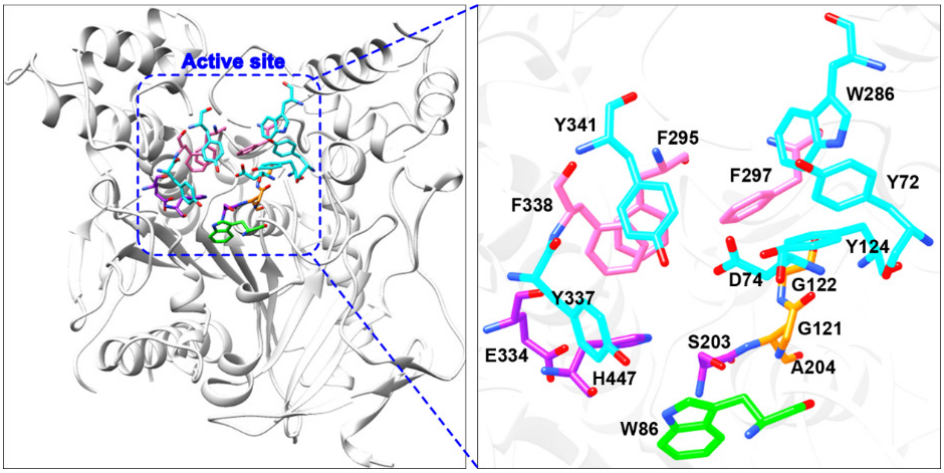

Figure 2 The binding regions of the *h*AChE active site gorge, including the residues of catalytic site (purple), anionic subsite (green), oxyanion hole (orange), acyl binding pocket (pink) and PAS (cyan).

Rational design of more potent *h*AChE inhibitors would be beneficial from a better understanding of how the current drugs bind to *h*AChE at the active site. As mentioned previously, 2 available anti-AD drugs, DPZ and GLM, are selective inhibitors of *h*AChE. Based on X-ray crystal structures, the crystallographic profile demonstrated that the DPZ piperidine moiety can bind to CAS of *h*AChE, while the DPZ indanone moiety is also able to interact with the PAS of *h*AChE, called dual-binding mode of *h*AChE inhibition. For *h*AChE/GLM complex, the whole part of GLM molecule can only bind to CAS of *h*AChE active site gorge [24]. The different binding modes between DPZ and GLM in the active site of *h*AChE led to the significant difference of inhibitory activity against the *h*AChE. The half maximal inhibitory concentration (IC_{50}) values taken from *in vitro* experiment showed that the inhibitory effect of DPZ (IC_{50} = 23.1 nM) on *h*AChE was about 85 times more potent than that of GLM (IC_{50} = 2,010 nM) [25]. However, the result from X-ray crystal structures could not explain the binding dynamics of both complexes in aqueous solution. Therefore, in the present study, we investigated the binding modes and dynamic behaviors of *h*AChE in complex with DPZ and GLM, which could lead to difference in their binding affinity using molecular dynamics (MD) simulation. For our simulations, the intermolecular hydrogen bonds, the per-residue free energy decomposition, and the binding free energy calculation were intensively analyzed. Our results provided a better understanding of the binding interactions between *h*AChE and its inhibitors. Besides, such information could be useful for future design of more potent *h*AChE inhibitors.

Materials and methods

System preparation

The staring geometries of the *h*AChE in complex with DPZ and GLM were obtained from the Protein Data Bank (PDB), entry codes 4EY7 and 4EY6, respectively [24]. The complexes were studied by MD simulations using AMBER12 software [26] with the AMBER ff03 force field [27]. The MD procedures were performed as follows. The missing hydrogen atoms of complex were added using the LEaP module of AMBER12. The ionizable amino acids, consisting of lysine (K), arginine (R), aspartic acid (D), glutamic acid (E) and histidine (H) were assigned using PROPKA 3.1 program [28]. Note that the 2 residues in catalytic site, E334 and H447, were ionized as the negatively charged glutamate and the neutral histidine with protonated δ-NH (HID type), respectively. Possible intramolecular disulfide bonds [29] were also applied for maintaining the stability of protein structure. Added hydrogen atoms were minimized by steepest descent (SD) of 2,000 steps, followed by conjugated gradient (CG) of 1,000 steps to relieve bad contact of hydrogen atoms. Each complex was immersed in a simulation box of TIP3P water molecules [30] with spacing distance of 10 Å from protein surface, and a chloride counterion was randomly added to keep the whole system neutral. The box dimensions of both systems were approximately set to 55×79×79 $Å^3$, while the number of total atoms was 48,021 and 47,396 atoms for the *h*AChE/DPZ and *h*AChE/GLM, respectively. Afterward, the minimization of water molecules alone was firstly performed and continued by the entire system minimization with the SD (2,000 steps) and CG (1,000 steps), respectively, to obtain the optimum conformation for MD simulations in the next step.

Force field development for inhibitor parameters

The partial atomic charges and empirical force field parameters for the atoms in 2 inhibitors were prepared by the standard procedure [31-33]. Briefly, the atomic coordinates of DPZ and GLM were added by hydrogen atoms based on the covalent bond hybridizations. Each inhibitor was optimized at the HF/6-31(d) level of theory using Gaussian09 program [34] to obtain the most stable structures. After the structure optimization step, the optimized geometry was calculated the electrostatic potential (ESP) charges around its molecule by HF/6-31G* method. The charge fitting calculation was used for evaluating the restrained electrostatic potential (RESP) charges of molecule using antechamber module of AMBER12 package. Afterwards, the molecular parameters of DPZ and GLM were taken from the parmchk module [35] in accordance with the generalized AMBER force field (GAFF) [36].

Molecular dynamics simulations

MD simulation of the two studied systems were performed by the AMBER12 program coupled with the SANDER module. The long-range electrostatic interactions were treated using the particle mesh Ewald (PME) summation method [37] with the cutoff value of 12 Å. The SHAKE procedure [38] was employed to constrain the bond length and angles involving hydrogen with a time step of 2 fs. Afterwards, each system was increased in temperature from 0 to 298 K during the 100 ps and further allowed to stay at constant 298 K for another 12 ns to obtain the production phase. The *NPT* ensemble

periodic boundary at constant pressure of 1 atm was used for simulation. The Berendsen weak coupling algorithm was applied to control temperature and pressure [39]. The trajectories were collected every 2 ps for MD analysis.

For analysis, the ptraj module of AMBER12 software package was used to explore the root mean square displacement (RMSD) and hydrogen bond occupancy between enzyme and inhibitor, while the per-residue decomposition of MM-GBSA binding free energy ($\Delta G_{\text{bind}}^{\text{residue}}$) and the total free energy of binding (ΔG_{bind}), as well as their energy components were calculated by MM-GBSA and MM-PBSA methods using the mm_pbsa module.

Binding free energy calculations

The Molecular Mechanics/Poisson-Boltzmann Surface Area (MM-PBSA) and Molecular Mechanics/Generalized Born Surface Area (MM-GBSA) methods were effectively employed to calculate the binding free energies of enzyme-inhibitor complex [40,41]. Herein, the free energies of the *h*AChE in complex with DPZ and GLM (ΔG_{bind}) were calculated from the difference between the free energy of the complex ($\Delta G_{\text{complex}}$), enzyme ($\Delta G_{\text{enzyme}}$) and inhibitor ($\Delta G_{\text{inhibitor}}$), as shown in Eq. (1).

$$\Delta G_{\text{bind}} = \Delta G_{\text{complex}} - \Delta G_{\text{enzyme}} - \Delta G_{\text{inhibitor}} \quad (1)$$

The total Gibbs free energy (ΔG) can be estimated from enthalpy term (ΔH) and entropic contribution ($-T\Delta S$), as outlined in Eq. (2).

$$\Delta G = \Delta H - T\Delta S \quad (2)$$

In solution, the ΔH term is the summation of the molecular mechanical binding energy in gas phase (ΔE_{MM}) and the solvation free energy (ΔG_{solv}). Therefore, the Eq. (2) can be approximated, as expressed in Eq. (3).

$$\Delta G = (\Delta E_{\text{MM}} + \Delta G_{\text{solv}}) - T\Delta S \quad (3)$$

The energy of molecular mechanics in gas phase, ΔE_{MM}, is comprised bonded energy (ΔE_{bonded}), the coulomb (ΔE_{ele}) and van der Waal interaction energies (ΔE_{vdW}), as shown in Eq. (4).

$$\Delta E_{\text{MM}} = \Delta E_{\text{bonded}} + \Delta E_{\text{ele}} + \Delta E_{\text{vdW}} \quad (4)$$

The free energy of solvation (ΔG_{solv}) is divided into polar and nonpolar solvation terms. The free energy of electrostatic component was computed by either the Poisson-Boltzman (PB) or the Generalized Born (GB) model with the dielectric constant values of 1 and 80 for the solute and the surrounding solvent, respectively, as expressed in Eq. (5).

$$\Delta G_{\text{solv}} = \Delta G_{\text{PB(GB)}} + \Delta G_{\text{SASA}} \quad (5)$$

The nonpolar solvation free energy term ($\Delta G_{\text{nonpolar}}$) is estimated from the surface accessible surface area (SASA) using hard-sphere atomic model with a probe radius of 1.4 Å, as shown in Eq. (6).

$$\Delta G_{\text{nonpolar}} = \gamma \cdot \text{SASA} + \beta \quad (6)$$

where the surface tension parameters, γ and β, with the values of 0.00542 kcal/mol·Å^2 and 0.92 kcal/mol, respectively, are calculated by linear regression of a set of small nonpolar molecules solvent free energy in water [42]. The entropy term ($T\Delta S$) for conformational entropy change of the 2 individual molecules upon complex formation was taken from the normal mode analysis [43], to compute the vibrational, translational and rotational entropies. It is worth noting that the extracted 200 MD trajectories from the last 5 ns of each simulated system were used for calculating binding free energies based on MM-PBSA/GBSA methods.

Additionally, the contribution of individual residue upon complexation process between protein and ligand was calculated using the MM-GBSA per-residue free energy decomposition ($\Delta G_{\text{bind}}^{\text{residue}}$) by only taking into account the MM and solvation energies without the entropic contribution.

Results and discussion

System stability

To briefly investigate the stability of the 2 studied *h*AChE/inhibitor complexes during MD simulation, the RMSD of each system relative to the initial energy minimized structure for complex backbone atoms was plotted *versus* simulation time, as depicted in **Figure 3**. The results showed that the RMSD values of backbone atoms for the *h*AChE/DPZ reached equilibrium ~4.5 ns and fluctuated at ~1.4 Å. Meanwhile, the equilibrium time and conformational fluctuation for the *h*AChE/GLM were found at ~6.7 ns and ~1.7 Å, respectively. It suggested that both complexes tended to reach equilibrium at approximately 7 ns. Therefore, it is reasonable to perform further structural analyses and binding free energy calculation based on the MD snapshots extracted from the last 5 ns (7 to 12 ns).

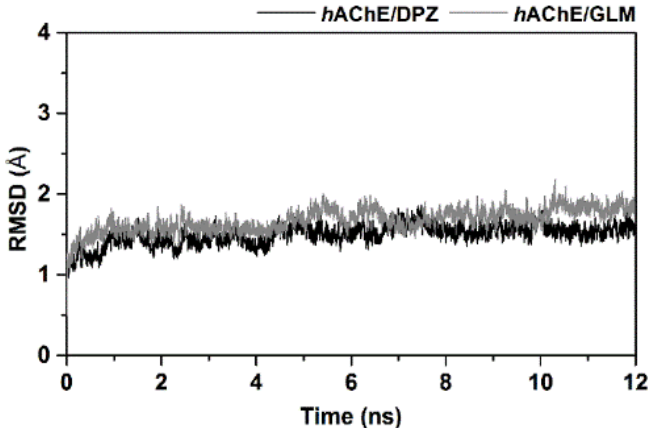

Figure 3 RMSD plots for the backbone atoms of the *h*AChE/DPZ (black) and *h*AChE/GLM (gray) complexes.

In addition, for better understanding on how DPZ and GLM binding affect the binding mode to *h*AChE, the structural changes between initial structure and the last MD snapshot of 2 complexes were examined. **Figure 4** highlighted that the conformations of DPZ and GLM exhibited a little movement, which meant that both drugs were stable throughout the MD simulation. Thus, this analysis indicated that *h*AChE/DPZ and *h*AChE/GLM complexes were relatively stable along simulation period as supported by the RMSD calculation mentioned above.

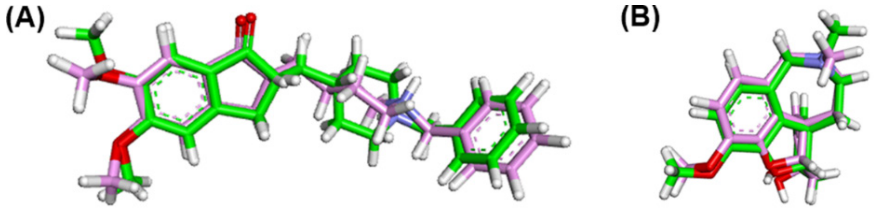

Figure 4 The superposition between initial structure (green) and the last MD snapshot (pink) for (**A**) DPZ and (**B**) GLM.

Intermolecular hydrogen bond of *h*AChE/inhibitor complex

Although the chemical structures of the 2 inhibitors studied here were different (**Figure 1**), they contain oxygen and nitrogen atoms, which could form intermolecular hydrogen bonds with the surrounding residues of *h*AChE at the active site gorge. To measure such interaction, hydrogen bonds can be calculated in terms of the percentage of hydrogen bond occupation in accordance with the 2 geometric criteria of (*i*) a proton donor (D) and acceptor (A) distance ≤ 3.5 Å and (*ii*) a D–H···A bond angle ≥ 120 º. The results are presented in **Table 1** and the schematic views of hydrogen bond interactions are given in **Figure 5**. It should be noted that hydrogen bond occupations with the values of > 75, 50 - 75 and < 50 % are defined as strong, medium and weak hydrogen bond interactions, respectively. Our findings indicated

that the *h*AChE in complex with DPZ had the higher percentage of hydrogen bond occupation than *h*AChE/GLM complex. The binding of *h*AChE to DPZ showed two strong hydrogen bonds (99 and 92 % occupancy) formed between –$^{+}$NH– group in piperidine ring of DPZ and nitrogen atom of H447 (NE2), as well as between carbonyl oxygen of DPZ and –NH– group of F295 backbone, respectively (**Figure 5(A)**). For *h*AChE/GLM complex, 1 medium hydrogen bond occupation (54 %) formed between hydroxyl group in cyclohexene moiety of GLM and oxygen atom in carbonyl group of H447 backbone (**Figure 5(B)**). The results reflected an importance of the catalytic residue H447 for binding of both drugs. These findings also suggested that the difference in percentage of hydrogen bond occupations for each complex could be one of an important reason, corresponding to the higher binding affinity of *h*AChE/DPZ than *h*AChE/GLM (discussed later). In addition, 2 weak hydrogen bonds (14 - 28 % occupancies, **Figure 5(C)**) were also found in *h*AChE/GLM complex, but they could be broken down by molecular orientation of GLM during simulation period (see below). The first weak interaction was the hydrogen bond between –$^{+}$NH– group in the azepine moiety of GLM and oxygen atom of D74 (OD2). The second interaction was the hydrogen bond between oxygen atom in benzene moiety of GLM and hydroxyl group of S203. Finally, the –$^{+}$NH– group in the azepine moiety of GLM formed a weak hydrogen bond with oxygen atom of D74 (OD1).

Table 1 Percentage of hydrogen bond occupations of *h*AChE in complex with DPZ and GLM during MD simulations.

System	Hydrogen bonding	% Hydrogen bond occupation
*h*AChE/DPZ	$^{+}$N–H···NE2@H447	99
	O···H–N@F295	92
*h*AChE/GLM	O–H···O@H447	54
	$^{+}$N–H···OD2@D74	28
	O···H–O@S203	14
	$^{+}$N–H···OD1@D74	14

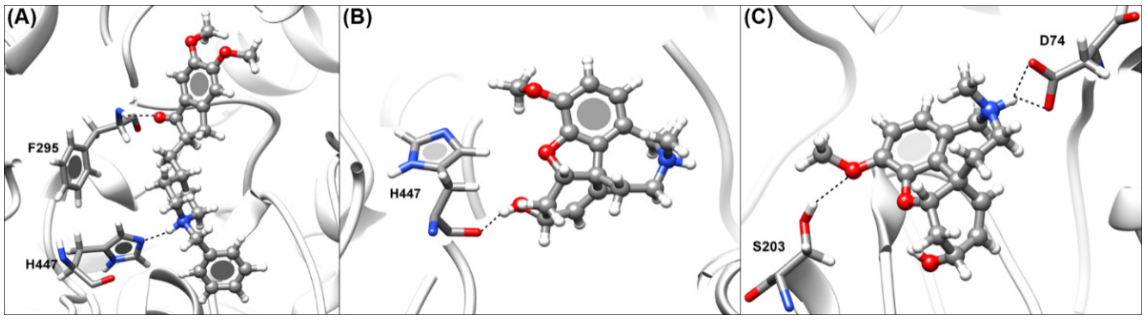

Figure 5 The schematic views of hydrogen bond interactions (dotted lines) demonstrated from the MD snapshots between the *h*AChE and its *h*AChE inhibitors for: (A) DPZ and (B) and (C) GLM.

To elucidate the hydrogen bonding formation relative to structural changes of GLM, the MD snapshots of *h*AChE/GLM at 4, 7 and 12 ns were visualized (**Figure 6**). The MD snapshots showed that the rotation of whole GLM molecule after 4 ns resulted in the breakdown of the 3 weak hydrogen bonds as mentioned previously. At the same time, the hydrogen bond with medium occupancy (defined as O–H···O@H447) could form instead till the end of simulation. This phenomenon culminated in the reduction of hydrogen bond occupancies of GLM to D74 and S203, which could be another reason resulting in the lower binding affinity of *h*AChE with GLM bound. Therefore, the results indicated that hydrogen bonding played an essential role in *h*AChE/inhibitor interaction, which affected inhibitory activity of both DPZ and GLM. In fact, the active site gorge of *h*AChE forms as hydrophobic cavity, and so other types of interactions need to be further determined.

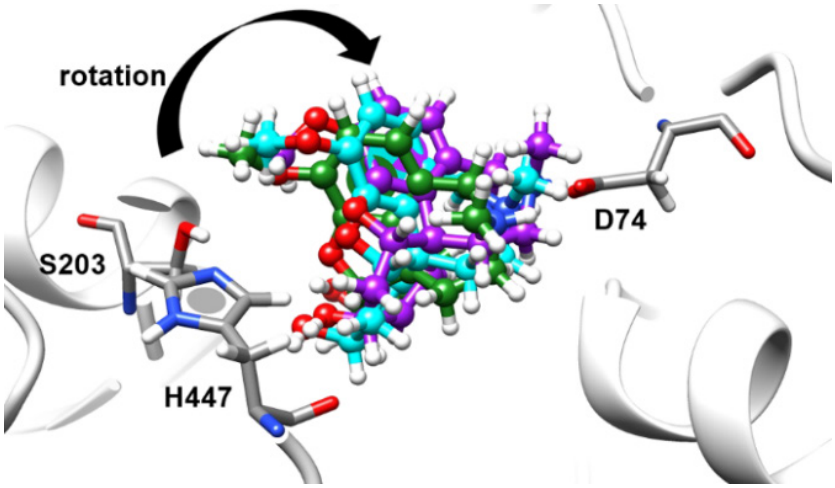

Figure 6 Sketch map for the molecular orientations of GLM extracted from MD snapshots at 4 ns (green), 7 ns (purple) and 12 ns (cyan).

Key residues for binding of *h*AChE/inhibitor complex

To pinpoint the key residues involved in inhibitor binding to *h*AChE, the calculation of per-residue free energy decomposition ($\Delta G_{\text{bind}}^{\text{residue}}$) based on MM-GBSA method was applied from the last 5 ns (7 - 12 ns). With an energy stabilization of less than −0.8 kcal/mol, the free energy from each residue showed that *h*AChE residues W86, G121, Y124, W286, V294, F295, F297, Y337, Y341 and H447 were considered as the stabilizing residues toward DPZ binding, as shown in **Figure 7(A)**. For *h*AChE/GLM complex, the major favorable free energy contributions predominately originated from the *h*AChE residues W86, G121, E202, F297, Y337, H447 and Y449 (**Figure 7(B)**). Meanwhile, the residues W86, G121, F297, Y337 and H447 were conserved for binding pattern of *h*AChE/inhibitor complex, where those of residues are mainly located at the CAS of *h*AChE. This finding supported the evidence from X-ray crystal structures by the fact that both DPZ and GLM bind to CAS of *h*AChE [24]. Moreover, only DPZ could interact with the residues in PAS of *h*AChE, including Y124, W286 and Y341, which was also consistent with X-ray crystal structure [24]. This could be appeared the third possible reason why *h*AChE/DPZ exhibited the higher binding affinity than *h*AChE/GLM. However, the residue E202 played a pivotal role in destabilization for binding of DPZ to *h*AChE by ~1.8 kcal/mol. This phenomenon was involved in the repulsive force between negatively charged E202 and benzyl moiety of DPZ, causing the reduced binding affinity of *h*AChE/DPZ. The result implied that the modification of DPZ benzyl moiety was most likely to improve the inhibitory effect of DPZ on *h*AChE. Interestingly, Kryger *et al.* [44] reported that the substitutions on the DPZ benzyl ring with a hydroxyl group substituent at the *para* position resulted in increased inhibitory effect. This was probably due to the forming of hydrogen bond between the residue E202 and the modified hydroxyl group.

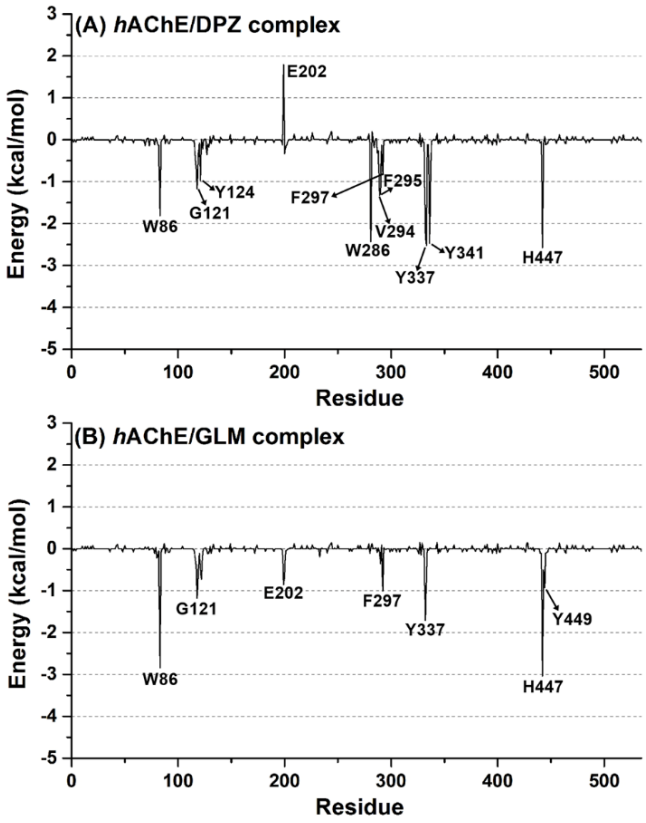

Figure 7 Per-residue free energy decomposition ($\Delta G_{\text{bind}}^{\text{residue}}$) of the *h*AChE in complex with (A) DPZ and (B) GLM.

To gain more understanding how the *h*AChE inhibitors with different chemical structures interact with amino acid residues in the enzyme active site. The degree of stabilization from individual stabilizing residue, including the other residues within 8-Å sphere surrounded by each inhibitor was separately considered the contributions from their backbone atoms ($\Delta G_{\text{bind}}^{\text{backbone}}$) and from side chain atoms ($\Delta G_{\text{bind}}^{\text{side chain}}$) in **Figure 8** (**left**), together with the electrostatic ($\Delta E_{\text{ele}} + \Delta G_{\text{polar}}$) and vdW ($\Delta E_{\text{vdW}} + \Delta G_{\text{nonpolar}}$) energies in **Figure 8** (**right**). Note that the focused residues were composed of 21 and 24 residues for *h*AChE/DPZ and *h*AChE/GLM, respectively. The results showed that most of the residues likely provided a degree of stabilization through their side chains, where the free energy from the residue atoms ($\Delta G_{\text{bind}}^{\text{residue}}$) was highly contributed from the side chain atoms in both complexes (**Figure 8**, **left**). This finding reflected an importance of *h*AChE side chain, participating in the binding of DPZ and GLM. However, this is except for the 3 residues G121, V294 and F295 for *h*AChE/DPZ, as well as the 2 residues G121 and H447 for *h*AChE/GLM, because the free energy from the backbone atoms played a stronger role. Besides, the 2 aromatic amino acids, W86 and Y337, were important for binding of DPZ and GLM through hydrophobic interaction. This is supported by the energy contribution of both residues primarily from the vdW term of < −2.0 kcal/mol (**Figure 8**, **right**). In addition, the *h*AChE side chains of aromatic residues Y124, W286, Y337 and Y341 located at PAS of *h*ACE active site created favorable vdW interactions to the indanone moiety of DPZ. This culminated in the inhibitory activity of *h*AChE/DPZ stronger than *h*AChE/GLM due to an additional interaction of DPZ indanone moiety to the residues in the PAS of *h*AChE. Hence, it suggested that GLM needed to be modified its structure, which could bind to the PAS of *h*AChE for increased binding affinity. Guilliou *et al.* [45] also reported that the modification of GLM into homo- or heterodimers showed the more potent inhibitory effect than that of the parent GLM by ~16 - 36 times. This is owing to the interactions between the residues in PAS of *h*AChE and the modified moieties of GLM. For the catalytic residue H447, it provided the degree of stabilization to DPZ binding through its side chain (–2.6 kcal/mol in **Figure 7A**, **left**) forming a strong hydrogen bond with the DPZ piperidine ring. This is strongly supported by the energy contribution of this residue from electrostatic term of –1.4 kcal/mol (**Figure 8A**, **left**). Whereas the backbone of H447 could

also interact with the hydroxyl group of GLM at the cyclohexene ring to form a medium hydrogen bond *via* electrostatic contribution of –2.3 kcal/mol (**Figure 8B**, **right**). Again, these results displayed an importance of the catalytic residue H447 for binding of DPZ and GLM associated with hydrogen bonding formation. There were no energy contributions from the rest of catalytic triad residues, S203 and E334 (data not shown); however, there was quite weak stabilization from the S203 side chain of –0.5 kcal/mol for *h*AChE/GLM complex (**Figure 8B**, **left**). Thus, the decomposition of the free energy on a per-residue basis was correlated well with the binding patterns of DPZ and GLM to *h*AChE.

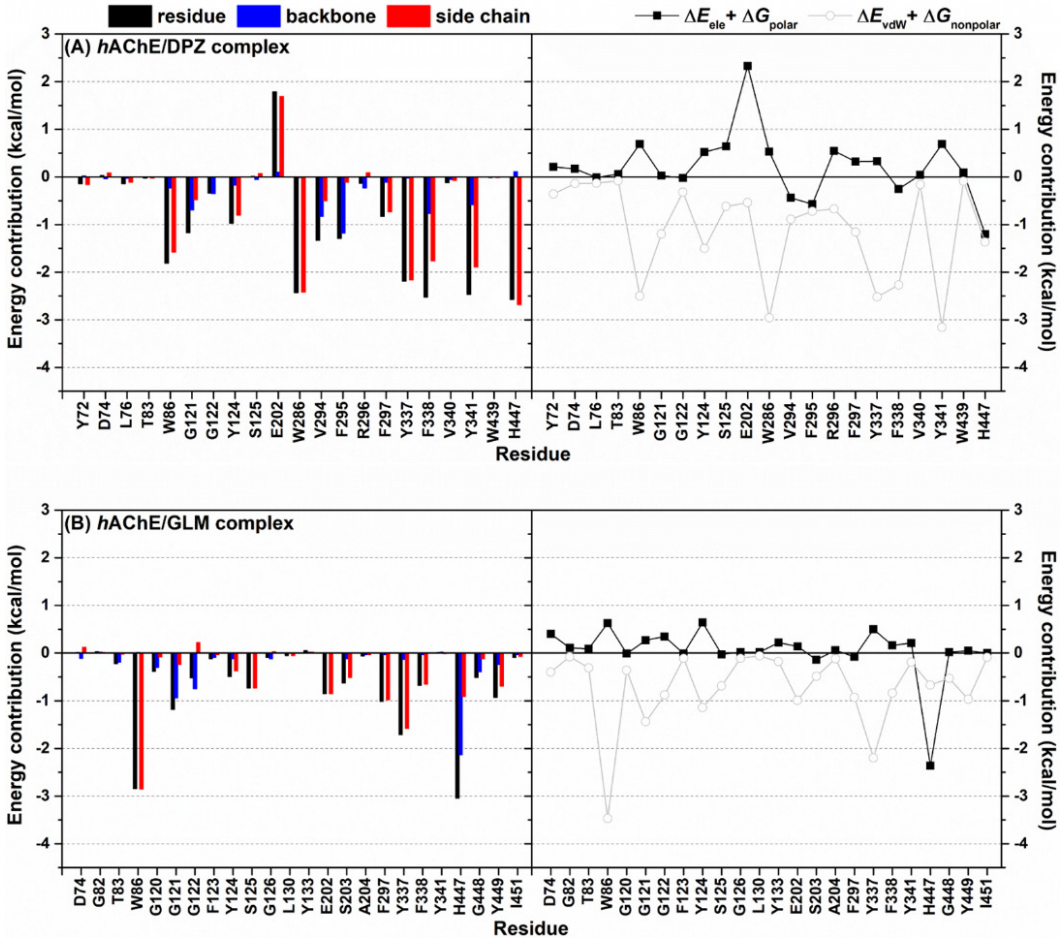

Figure 8 (**left**) Energy contributions from the residue, backbone and side chain of the *h*AChE in complex with (A) DPZ and (B) GLM. (**right**) Polar ($\Delta E_{ele} + \Delta G_{polar}$) and nonpolar ($\Delta E_{vdW} + \Delta G_{nonpolar}$) energy contributions from each residue of *h*AChE.

Binding free energy calculations

To estimate the free energies of complex in solution, the MM-PB(GB)SA energetic method was performed. A total 200 MD snapshots extracted from the last 5 ns of the production phase with the same set as those used for calculating the per-residue free energy decomposition were applied to calculate the total binding free energy of *h*AChE/inhibitor complexes. The free energy of binding (ΔG_{bind}) and the relevant energy components are summarized in **Table 2**.

Table 2 Binding free energy (kcal/mol) and its energetic components for *h*AChE/DPZ and *h*AChE/GLM complexes, as well as the experimental IC_{50} (nM) values from the 2 studied inhibitors binding to *h*AChE.

	DPZ		**GLM**	
	MM-PBSA	**MM-GBSA**	**MM-PBSA**	**MM-GBSA**
ΔE_{ele}	–148.6 ± 6.8		–119.5 ± 8.0	
ΔE_{vdW}	–55.6 ± 2.2		–37.8 ± 2.1	
ΔE_{MM}	–204.2 ± 7.0		–157.3 ± 7.9	
$\Delta G_{\mathrm{nonpolar,solv}}$	–6.5 ± 0.1	–6.3 ± 0.1	–5.0 ± 0.1	–4.9 ± 0.1
$\Delta G_{\mathrm{ele,solv}}$	168.5 ± 7.4	160.7 ± 6.7	138.8 ± 8.4	131.6 ± 8.1
ΔG_{solv}	162.1 ± 7.4	154.4 ± 6.7	133.8 ± 8.4	126.7 ± 8.0
$\Delta G_{\mathrm{ele,solv}} + \Delta E_{\mathrm{ele}}$	19.9 ± 4.2	12.1 ± 2.0	19.2 ± 4.0	12.1 ± 8.0
$\Delta G_{\mathrm{nonpolar,solv}} + \Delta E_{\mathrm{vdW}}$	–62.1 ± 1.2	–61.9 ± 1.2	–42.8 ± 1.1	–42.7 ± 1.1
$\Delta G_{\mathrm{total}}$	–42.2 ± 4.7	–49.8 ± 3.0	–23.5 ± 3.9	–30.6 ± 2.3
$-T\Delta S$	21.9 ± 11.8		15.4 ± 7.2	
ΔG_{bind}	–20.3 ± 8.2	–27.9 ± 7.4	–8.1 ± 5.6	–15.2 ± 4.8
IC_{50} (nM)	23.1 ± 4.8		2,010 ± 150	
[a]$\Delta G_{\mathrm{bind}}^{\mathrm{exp}}$	–10.4		–7.8	

[a]The experimental value of binding free energy ($\Delta G_{\mathrm{bind}}^{\mathrm{exp}}$) was calculated from IC_{50} values using the formula $\Delta G_{\mathrm{bind}} \approx RT\ ln\ I\ C_{50}$, where $R = 1.987 \times 10^{-3}$ kcal/mol, T = 298 K, and IC_{50} was expressed in M. IC_{50} values of DPZ and GLM were obtained from Bolognesi *et al.* [25].

The binding free energy calculation suggested that the preferential attractive electrostatic interactions in gas phase (ΔE_{ele}) of *h*AChE/GLM (–119.5 kcal/mol) and *h*AChE/DPZ (–148.8 kcal/mol) were greater than the vdW energy (–37.8 for *h*AChE/GLM and –55.6 kcal/mol for *h*AChE/DPZ) by ~3-fold, as shown in **Table 2**. This was corresponded to the order of the percentage of hydrogen bond occupations, in which the *h*AChE/DPZ had the higher hydrogen bond occupancies than *h*AChE complexed with GLM. Considering the free energy combined with solvation free energy, the polar term ($\Delta G_{\mathrm{ele,solv}} + \Delta E_{\mathrm{ele}}$) was an unfavorable contribution, which was determined to a large extent by desolvation energy with relatively high positive values of polar solvation resulting from either PB or GB models in both complexes. This phenomenon has been also found in some biological systems in an aqueous solution, where the binding pocket of enzyme is a hydrophobic cavity [46,47]. On the other hand, the nonpolar solvation term ($\Delta G_{\mathrm{nonpolar,solv}} + \Delta E_{\mathrm{vdW}}$) showed more favorable contribution to the total binding free energies in both complexes. These findings suggested that both vdW interaction and nonpolar solvation are the key driving force for binding of DPZ and GLM to *h*AChE. Besides, it implied that the design of novel *h*AChE inhibitors with the higher hydrophobicity than DPZ and GLM might increase inhibitory effect of inhibitors toward *h*AChE. With a summation of the entropic contribution ($-T\Delta S$), the MM-PBSA and MM-GBSA-based binding free energy of *h*AChE/DPZ (–20.3 and –27.9 kcal/mol) was stronger than *h*AChE/GLM (–8.1 and –15.2 kcal/mol), which agreed well with the experimentally determined inhibitory effects. It should be mentioned that, although in this study the binding free energies from either MM-PBSA or MM-GBSA method do not provide the accurately absolute experimental values of binding free energy, both approaches could be used for comparing experimental data quite well. In good accordance with Hou *et al.* [48], the calculated binding free energy from MM-PBSA method was highly close to the experimental data rather than the MM-GBSA method. This is based on the fact that the PB model is theoretically more rigorous than the GB model, and therefore MM-PBSA is usually considered to be naturally superior to MM-GBSA for calculation of the binding free energies of protein - ligand complex.

Conclusions

In this research, 12-ns MD simulations were conducted to determine dynamics behavior and binding affinity of 2 existing anti-AD drugs, DPZ and GLM, toward *h*AChE. The results revealed that both drugs directly interact with the catalytic residue H447 *via* hydrogen bonding formation. However, the molecular rotation of GLM during MD simulation deceases hydrogen bond occupancies of D74 and S203 to GLM binding, leading to the lower susceptibility of *h*AChE/GLM than *h*AChE/DPZ. Scanning of the per-residue free energy decomposition suggested that the binding of DPZ and GLM to *h*AChE is favorably stabilized by most of the residues in CAS (*i.e.*, W86, G121, F297 and H447). Only DPZ complex displays an additional interaction between DPZ and the residues in PAS of *h*AChE as expected. This could be considered as one of the possible reasons of the greater inhibitory activity of *h*AChE/DPZ than *h*AChE/GLM. Nonetheless, the reduced binding affinity of *h*AChE/DPZ is probably caused by the repulsive interaction between the negatively charged E202 and benzyl moiety of DPZ. The MM-PB(GB)SA-based binding free energy indicated that the vdW interactions are the main driving force for the binding in both complexes. Taken altogether, the protein - ligand interactions and the calculated total binding free energies supported the stronger binding affinity of *h*AChE/DPZ as compared to *h*AChE/GLM, which is in excellent agreement with the experimental data. Therefore, our computational information presented here could be useful for further design of more efficient *h*AChE inhibitors.

Acknowledgements

This research project was supported by Faculty of Science, Mahidol University, Thailand.

References

[1] Alzheimer's Association. 2020 Alzheimer's disease facts and figures. *Alzheimer's Dement.* 2020; **16**, 391-460.
[2] MW Bondi, EC Edmonds and DP Salmon. Alzheimer's disease: Past, present, and future. *J. Int. Neuropsychol. Soc.* 2017; **23**, 818-31.
[3] M Giri, M Zhang and Y Lü. Genes associated with Alzheimer's disease: An overview and current status. *Clin. Interv. Aging.* 2016; **11**, 665-81.
[4] JM Long and DM Holtzman. Alzheimer disease: An update on pathobiology and treatment strategies. *Cell* 2019; **179**, 312-39.
[5] MVF Silva, CMG Loures, LCV Alves, LC de Souza, KBG Borges and MG Carvalho. Alzheimer's disease: Risk factors and potentially protective measures. *J. Biomed. Sci.* 2019; **26**, 33.
[6] EE Congdon and EM Sigurdsson. Tau-targeting therapies for Alzheimer disease. *Nat. Rev. Neurol.* 2018; **14**, 399-415.
[7] F Panza, M Lozupone, G Logroscino and BP Imbimbo. A critical appraisal of amyloid-β-targeting therapies for Alzheimer disease. *Nat. Rev. Neurol.* 2019; **15**, 73-88.
[8] CM Henstridge, BT Hyman and TL Spires-Jones. Beyond the neuron - cellular interactions early in Alzheimer disease pathogenesis. *Nat. Rev. Neurosci.* 2019; **20**, 94-108.
[9] TH Ferreira-Vieira, IM Guimaraes, FR Silva and FM Ribeiro. Alzheimer's disease: Targeting the cholinergic system. *Curr. Neuropharmacol.* 2016; **14**, 101-15.
[10] A Sanabria-Castro, I Alvarado-Echeverría and C Monge-Bonilla. Molecular pathogenesis of Alzheimer's disease: An update. *Ann. Neurosci.* 2017; **24**, 46-54.
[11] K Sharma. Cholinesterase inhibitors as Alzheimer's therapeutics (Review). *Mol. Med. Rep.* 2019; **20**, 1479-87.
[12] R León, AG Garcia and J Marco-Contelles. Recent advances in the multitarget-directed ligands approach for the treatment of Alzheimer's disease. *Med. Res. Rev.* 2013; **33**, 139-89.
[13] R Cacabelos. Donepezil in Alzheimer's disease: From conventional trials to pharmacogenetics. *Neuropsychol. Dis. Treat.* 2007; **3**, 303-33.
[14] DA Casey, D Antimisiaris and J O'Brien. Drugs for Alzheimer's disease: Are they effective? *Pharma. Therapeut.* 2010; **35**, 208-11.
[15] A Nordberg, T Darreh-Shori, E Peskind, H Soininen, M Mousavi, G Eagle and R Lane. Different cholinesterase inhibitor effects on CSF cholinesterases in Alzheimer patients. *Curr. Alzheimer Res.* 2009; **6**, 4-14.
[16] H Sugimoto, H Ogura, Y Arai, Y Iimura and Y Yamanishi. Research and development of donepezil hydrochloride, a new type of acetylcholinesterase inhibitor. *Jpn. J. Pharmacol.* 2002; **89**, 7-20.

[17] LJ Scott and KL Goa. Galantamine: A review of its use in Alzheimer's disease. *Drugs* 2000; **60**, 1095-122.
[18] MCR Simoes, FPD Viegas, MS Moreira, MDF Silva, MM Riquiel, PMD Rosa, MR Castelli, MHD Santos, MG Soares and C Viegas. Donepezil: An important prototype to the design of new drug candidates for Alzheimer's disease. *Mini Rev. Med. Chem.* 2014; **14**, 2-19.
[19] JL Sussman, M Harel, F Frolow, C Oefner, A Goldman, L Toker and I Silman. Atomic structure of acetylcholinesterase from Torpedo californica: A prototypic acetylcholine-binding protein. *Science* 1991; **253**, 872-9.
[20] H Dvir, I Silman, M Harel, TL Rosenberry and JL Sussman. Acetylcholinesterase: From 3D structure to function. *Chem. Biol. Interact.* 2010; **187**, 10-22.
[21] A Ordentlich, D Barak, C Kronman, N Ariel, Y Segall, B Velan and A Shafferman. Functional characteristics of the oxyanion hole in human acetylcholinesterase. *J. Biol. Chem.* 1998; **273**, 19509-17.
[22] TL Rosenberry, X Brazzolotto, IR MacDonald, M Wandhammer, M Trovaslet-Leroy, S Darvesh and F Nachon. Comparison of the binding of reversible inhibitors to human butyrylcholinesterase and acetylcholinesterase: A crystallographic, kinetic and calorimetric study. *Molecules* 2017; **22**, 2098.
[23] G Johnson and SW Moore. The peripheral anionic site of acetylcholinesterase: Structure, functions and potential role in rational drug design. *Curr. Pharmaceut. Des.* 2006; **12**, 217-25.
[24] J Cheung, MJ Rudolph, F Burshteyn, MS Cassidy, EN Gary, J Love, MC Franklin and JJ Height. Structures of human acetylcholinesterase in complex with pharmacologically important ligands. *J. Med. Chem.* 2012; **55**, 10282-6.
[25] ML Bolognesi, R Banzi, M Bartolini, A Cavalli, A Tarozzi, V Andrisano, A Minarini, M Rosini, V Tumiatti, C Bergamini, R Fato, G Lenaz, P Hrelia, A Cattaneo, M Recanatini and C Melchiorre. Novel class of quinone-bearing polyamines as multi-target-directed ligands to combat Alzheimer's disease. *J. Med. Chem.* 2007; **50**, 4882-97.
[26] R Salomon-Ferrer, DA Case and RC Walker. An overview of the Amber biomolecular simulation package. *Wires Comput. Mol. Sci.* 2013; **3**, 198-210.
[27] Y Duan, C Wu, S Chowdhury, MC Lee, G Xiong, W Zhang, R Yang, P Cieplak, R Luo, T Lee, J Caldwell, J Wang and P Kollman. A point-charge force field for molecular mechanics simulations of proteins based on condensed-phase quantum mechanical calculations. *J. Comput. Chem.* 2003; **24**, 1999-2012.
[28] MHM Olsson, CR Søndergaard, M Rostkowski and JH Jensen. PROPKA3: Consistent treatment of internal and surface residues in empirical pKa predictions. *J. Chem. Theor. Comput.* 2011; **7**, 525-37.
[29] J Wiesner, Z Kříž, K Kuča, D Jun and J Koča. Acetylcholinesterases - the structural similarities and differences. *J. Enzym. Inhib. Med. Chem.* 2007; **22**, 417-24.
[30] WL Jorgensen, J Chandrasekhar, JD Madura, RW Impey and ML Klein. Comparison of simple potential functions for simulating liquid water. *J. Chem. Phys.* 1983; **79**, 926-35.
[31] P Mahalapbutr, P Chusuth, N Kungwan, W Chavasiri, P Wolschann and T Rungrotmongkol. Molecular recognition of naphthoquinone-containing compounds against human DNA topoisomerase IIα ATPase domain: A molecular modeling study. *J. Mol. Liq.* 2017; **247**, 374-85.
[32] W Panman, B Nutho, S Chamni, S Dokmaisrijan, N Kungwan and T Rungrotmongkol. Computational screening of fatty acid synthase inhibitors against thioesterase domain. *J. Biomol. Struct. Dynam.* 2018; **36**, 4114-25.
[33] K Sanachai, P Mahalapbutr, K Choowongkomon, RP Poo-Arporn, P Wolschann and T Rungrotmongkol. Insights into the binding recognition and susceptibility of tofacitinib toward janus kinases. *ACS Omega* 2020; **5**, 369-77.
[34] MJ Frisch, GW Trucks, HB Schlegel, GE Scuseria, MA Robb, JR Cheeseman, G Scalmani, V Barone, B Mennucci, GA Petersson, H Nakatsuji, M Caricato, X Li, HP Hratchian, AF Izmaylov, J Bloino, G Zheng, JL Sonnenberg, M Hada, …, DJ Fox. Gaussian 09; Gaussian, Inc. *Wallingford CT* 2009; **32**, 5648-52.
[35] J Wang, W Wang, PA Kollman and DA Case. Automatic atom type and bond type perception in molecular mechanical calculations. *J. Mol. Graph. Model.* 2006; **25**, 247-60.
[36] J Wang, RM Wolf, JW Caldwell, PA Kollman and DA Case. Development and testing of a general amber force field. *J. Comput. Chem.* 2004; **25**, 1157-74.

[37] DM York, TA Darden and LG Pedersen. The effect of long-range electrostatic interactions in simulations of macromolecular crystals: A comparison of the Ewald and truncated list methods. *J. Chem. Phys.* 1993; **99**, 8345-8.
[38] JP Ryckaert, G Ciccotti and HJC Berendsen. Numerical integration of the cartesian equations of motion of a system with constraints: Molecular dynamics of n-alkanes. *J. Comput. Phys.* 1977; **23**, 327-41.
[39] HJC Berendsen, JPM Postma, WF van Gunsteren, A DiNola and JR Haak. Molecular dynamics with coupling to an external bath. *J. Comput. Phys.* 1984; **81**, 3684-90.
[40] C Wang, D Greene, L Xiao, R Qi and R Luo. Recent developments and applications of the MMPBSA method. *Front. Mol. Biosci*. 2018; **4**, 87.
[41] E Wang, H Sun, J Wang, Z Wang, H Liu, JZH Zhang and T Hou. End-point binding free energy calculation with MM/PBSA and MM/GBSA: Strategies and applications in drug design. *Chem. Rev.* 2019; **119**, 9478-508.
[42] H Gohlke and DA Case. Converging free energy estimates: MM-PB(GB)SA studies on the protein - protein complex Ras - Raf. *J. Comput. Chem.* 2004; **25**, 238-50.
[43] F Tama and YH Sanejouand. Conformational change of proteins arising from normal mode calculations. *Protein Eng.* 2001; **14**, 1-6.
[44] G Kryger, I Silman and JL Sussman. Structure of acetylcholinesterase complexed with E2020 (Aricept®): Implications for the design of new anti-Alzheimer drugs. *Structure* 1999; **7**, 297-307.
[45] C Guillou, A Mary, DZ Renko, E Gras and C Thal. Potent acetylcholinesterase inhibitors: Design, synthesis and structure-activity relationships of alkylene linked bis-galanthamine and galanthamine-galanthaminium salts. *Bioorg. Med. Chem. Lett.* 2000; **10**, 637-9.
[46] W Innok, A Hiranrat, N Chana, T Rungrotmongkol and P Kongsune. *In silico* and *in vitro* anti-AChE activity investigations of constituents from Mytragyna speciosa for Alzheimer's disease treatment. *J. Comput. Aid. Mol. Des.* 2021; **35**, 325-36.
[47] B Nutho, P Mahalapbutr, K Hengphasatporn, NC Pattaranggoon, N Simanon, Y Shigeta, S Hannongbua and T Rungrotmongkol. Why are lopinavir and ritonavir effective against the newly emerged coronavirus 2019? Atomistic insights into the inhibitory mechanisms. *Biochemistry* 2020; **59**, 1769-79.
[48] T Hou, J Wang, Y Li and W Wang. Assessing the performance of the MM/PBSA and MM/GBSA methods. 1. The accuracy of binding free energy calculations based on molecular dynamics dimulations. *J. Chem. Inform. Model.* 2010; **51**, 69-82.